Optimal Control of Convective Drying of Saturated Porous Materials

S. J. Kowalski, A. Rybicki, and K. Rajewska
Poznań University of Technology, Institute of Technology and Chemical Engineering, Dept. of Process Engineering, 60-965 Poznań, Poland

DOI 10.1002/aic.14225
Published online September 19, 2013 in Wiley Online Library (wileyonlinelibrary.com)

Numerical simulations of optimal control applied to saturated capillary-porous materials subjected to convective drying are presented. The optimization process is concerned with such drying parameters as drying rate, energy consumption, and product quality. The thermo-hydro-mechanical model of drying is developed to describe the kinetics of drying and to determine the drying-induced stresses which are responsible for damage of dried products. The effective and the admissible stresses are defined and used to formulate the Huber-von Mises–Hencky strength criterion enabling assessment of possible material damage. The method of genetic algorithm is used for operation with drying conditions in such a way as to ensure minimum energy consumption and to get the effective stress less than the strength of dried material, and thus, to preserve a good quality of dried products at possibly high drying rate. Numerically simulated optimal drying processes are illustrated on the examples of finite dimensions of kaolin-clay cylinders subjected to convective drying.
 AIChE J, 59: 4846–4857, 2013
Keywords: drying control, modeling, numerical simulation, porous materials, stresses, damage

Introduction

Drying rate, energy consumption, and quality of dried products constitute the three common quantities usually considered for the assessment of drying effectiveness.[1–4] Numerical simulation of drying processes and their optimal control with respect to these three quantities is presented in this article. It is possible to control drying rate or drying time on the basis of drying kinetics, or strictly, the so called drying curves.[5] It is possible to assess the net energy consumption used for heating of drying body and for evaporation of moisture on the basis of drying kinetics determined experimentally and correlated with the theoretical one followed up from the respective drying model.[6] The quality of a capillary-porous material after drying is stated as satisfactory if the products do not sustain damage, that is, if the drying induced stresses do not cause cracking or fracture of the products.[7–13] This mechanical effect is controlled by comparison of the Huber-von Mises–Hencky strength criterion with the admissible stress prescribed for the material at hand.

The distribution and time evolution of temperature, moisture content, and stresses in convectively dried material are determined on the basis of a thermo-hydro-mechanical model developed earlier by Kowalski.[14] The state of drying materials is determined and controlled in such a way as to make the drying process effective, that is, to assure high drying rate, minimum energy consumption, and good quality (no cracks) of dried products. The optimization procedure is illustrated on the kaolin-clay material in the form of cylindrical samples. The cylindrical form of the samples is used for convenience in both experimental and numerical tests as well as for theory validation.

The genetic algorithm method[15] is used in this article to simulate the optimal work of the dryer. This optimization method is realized through programming of the computer memory in such a way as to obtain a prescribed goal. A chain of directives consisting of zeros and units are used to code a prescription for getting the best solution of the optimized problem. The action of the genetic algorithm consists of multiple repetition of the following actions: estimation of adjustment (looking for the maximal value), selection (choice of the element which is the most profitable for the problem at hand), crossbreeding (creation of a new element from two elements originating from different populations), mutation (change of a single element randomly chosen), and modification of initial population (replacing an initial element by a new one if the latter is better). Next, the genetic algorithm comes back to the "selection" point and the procedure is repeated again to get finally a satisfactory result. The work of the ventilator and the heater in the drying set up was coded in such a way as to enable their usage in our considerations.

The elaboration of optimized drying processes with respect to drying rate, energy consumption, and quality of dried products is based on the thermo-hydro-mechanical model of drying shortly presented in the section to follow.

Modeling

The drying model applied in this article is accomplished under the following assumptions[16–24]

Correspondence concerning this article should be addressed to: K. Rajewska at kinga.rajewska@put.poznan.pl.

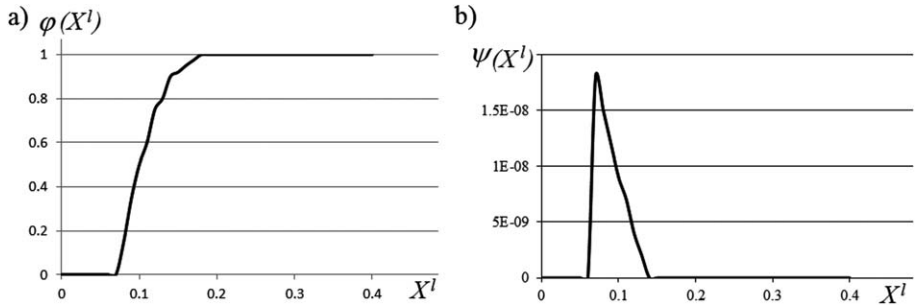

Figure 1. Graphical illustration: (a) the liquid mobility coefficient, (b) the phase transition coefficient, as a function of liquid content in drying body.

- The dried material is an isotropic capillary-porous body containing pores in an immiscible liquid-gas (vapor) mixture.
- The body is deformable, however, the strains are assumed to be small and their influence on the heat and mass transfer is negligible.
- The phase transition of liquid into vapor proceeds close to the thermodynamic equilibrium state, and the temperature of the moisture and the skeleton in a given point of the body are the same.
- The energy supplied to drying body due to microwave radiation is proportional to the local moisture content at a given moment.
- The stress in the moisture is represented simply by the moisture pressure.
- The material coefficients existing in the equations of mathematical model are, in general, functions of temperature and moisture content in the liquid phase. The influence of gas phase on body deformations and material shrinkage is considered as insignificant.
- The drying process is considered as a quasistatic one, that is, thermal and pressure shocks are excluded.

Moisture content

As it was assumed above, the moisture content in liquid phase is the main parameter which decides on the mechanical behavior of the body under drying. To develop the differential equation describing the mapping of liquid content in drying body, the following balance of liquid mass is used[14]

$$\rho^{\mathrm{s}}\dot{X}^l = -\operatorname{div}\boldsymbol{W}^l + \hat{\rho}^1 \tag{1}$$

where $X^l = \rho^1/\rho^{\mathrm{s}}$ is the liquid content referred to the mass of dry body, ρ^{s} and ρ^1 denote the mass concentration (mass per unit volume) of the solid skeleton and liquid, $\boldsymbol{W}^l$ is the liquid flux with respect to skeleton (amount of liquid per unit area and unit time), and $\hat{\rho}^1$ denotes the rate of liquid transition into vapor. Dot over symbols denotes the substantial time derivative.

Based on the thermodynamic rules, it was concluded[14] that the moisture flux is proportional to the gradient of chemical potential μ^l, which is a function of local parameters of state such as: temperature T, strain of the porous body ε, and the liquid content X^l. In accordance with the above formulated assumptions, we neglect the influence of small strains on moisture transport, and write

$$\boldsymbol{W}^l = -\Lambda^l \operatorname{grad}\mu^l\left(T, X^l\right) \tag{2}$$

where $\Lambda^l(T, X^l)$ is termed the liquid transport coefficient (mobility) defined as follows[25–27]

$$\Lambda^l\left(T, X^l\right) = \frac{\sigma(T)}{\eta(T)} f\left(X^l\right) \tag{3}$$

Here, $\sigma(T) = 75[1 - 0.002(T - 273)]$ is the surface tension of liquid on the interphase liquid/solid, $\eta(T) = \eta_0/[1 + 0.053(T - 273)]$ is the liquid viscosity with $\eta_0 = 183{\cdot}10^{-5}$ (Pa s), and $f(X^l)$ is a parameter dependent on pore structure and liquid content.[27]

In several stages of drying, the parameter $f(X^l)$ is suggested to be of the form

$$\frac{f\left(X^l\right)}{f_0} = \begin{cases} 1 & \text{dla } X^l \geq X_{cr} \\ \varphi\left(X^l\right) & \text{dla } X_{\mathrm{eq}} \leq X^l \leq X_{cr} \\ 0 & \text{dla } X^l \leq X_{\mathrm{eq}} \end{cases} \tag{4}$$

where X_{cr} and X_{eq} denote the critical and the equilibrium (final) moisture contents.

It was assumed here that the parameter $f(X^l)$ is constant and equal to f_{o} above the critical moisture content X_{cr}. Below the equilibrium moisture content X_{eq} the liquid motion disappears, so that $f(X^l) = 0$. For the moisture content in the range $X_{\mathrm{eq}} < X^l < X_{\mathrm{cr}}$, which corresponds to the falling drying rate period (FDRP), the liquid mobility is described by a continuously decreasing function of liquid content $\phi(X^l)$ (Figure 1a).

The rate of liquid change due to phase transition is assumed to be proportional to the difference between chemical potentials of liquid $\mu^l(T, X^l)$ and vapor $\mu^v(T, X^v)$, that is[14]

$$\hat{\rho}^1 = -\hat{\rho}^v = -\varpi\left(T, X^l\right)\left(\mu^l - \mu^{\mathrm{v}}\right) \tag{5}$$

where $\varpi\left(T, X^l\right)$ is the phase transition coefficient dependent on temperature and liquid content.

Here, we examine the drying body behavior until the moisture in liquid form is totally removed. This is because only the changes in liquid content involve shrinkage and generate stresses causing cracks of dried body. The changes in body temperature during drying are not so meaningful and hence, insignificantly influence the body deformations. It was assumed that the drying process considered here is a quasistatic one and proceeds close to the thermodynamic equilibrium, which means that the chemical potentials of liquid and vapor differ only slightly from each other. Then, we can write

$$\mu^v = [1 - \kappa(T)]\mu^l\left(X^l, T\right) \text{ and } \hat{\rho}^l = -\omega\left(X^l, T\right)\mu^l\left(X^l, T\right) \tag{6}$$

where $0 \leq \kappa < 1$ is a ratio termed further as the coefficient of phase transition efficiency (in thermodynamic equilibrium $\kappa = 0$), and $\omega\left(X^l, T\right) = \kappa(T)\varpi\left(X^l, T\right)$ is the intensity of phase transitions.

We assume that in the constant drying rate period (CDRP), the phase transition takes place mainly at the body surface, where the evaporation proceeds as if from the free liquid surface. The phase transitions inside the body in this period are assumed as insignificant. The phase transitions inside the body are of huge importance in the FDRP, so the phase transition intensity is assumed to be of the form

$$\frac{\omega(T,X)}{\omega_0(T)}=\begin{cases}0 & \text{dla } X\geq X_{cr}\\ \psi\left(X^l\right) & \text{dla } X_{\text{eq}}\leq X^l\leq X_{cr}\\ 0 & \text{dla } 0\leq X^l\leq X_{\text{eq}}\end{cases} \tag{7}$$

Similarly as in the case of moisture mobility, the phase transition of liquid into vapor in the range $X_{\text{eq}}<X^l<X_{\text{cr}}$ corresponding to the FDRP is described by a continuous function of liquid content $\psi(X^l)$[4,26] (Figure 1b).

Based on Eqs. 1 and 2 and the relation 5, and making use of the developed form of liquid potential $\mu^l(T, X^l)$ with respect to parameters $T=T_{\text{r}}+\vartheta$ and $X^l=X_r^l+\theta$, we can write the differential equation describing the distribution and time evolution of liquid content in drying body

$$\rho^s\dot{\theta}^l=\Lambda^l\nabla^2[c_T\vartheta+c_X\theta]-\omega[c_T\vartheta+c_X\theta] \tag{8}$$

where $\vartheta=T-T_r$ and $\theta=X^l-X_r^l$ denote the difference of temperature and liquid content with respect to some reference state. Coefficients c_T and c_X express the derivatives of chemical potential $\mu^l(T, X^l)$ with respect to temperature and liquid content, respectively, and can be interpreted as thermodiffusional and diffusional coefficients contributing to the liquid motion inside the body. Recalling the assumption that drying processes run quasistatically, we have neglected in Eq. 8, the expression $\text{grad}\,\Lambda^l\cdot\text{grad}\,\mu^l\approx 0$ as small and insignificant.

Temperature

A differential equation describing the mapping of temperature in dried body is developed from the balance of energy, which is of the form[28–30]

$$\rho^s\dot{s}T=-\text{div}\left[\boldsymbol{q}+\left(Ts^l\boldsymbol{W}^l+Ts^v\boldsymbol{W}^v\right)\right] \tag{9}$$

where $s(T,\ X^l,\ X^v)=s^s+s^l\ X^l+s^v\ X^v$ denotes the total entropy of drying body referred to the mass of dry body, s^α is the entropy of constituent α, $\boldsymbol{q}$ is the heat flux supplied through the body surface, and $\boldsymbol{W}^\alpha$ is the mass flux of constituent α.

Equation 9 expresses time changes of entropy caused by the heat supplied to the body due to conduction and heat transported with mass fluxes.

The heat flux is then written as follows[14]

$$\boldsymbol{q}=-\Lambda_T\text{grad}\,T-\left(Ts^l\boldsymbol{W}^l+Ts^v\boldsymbol{W}^v\right)] \tag{10}$$

where $\Lambda_T(T, X^l)$ is the coefficient of thermal conductivity per unit mass of the solid, and is expressed as a combination of thermal conductivity in the skeleton Λ_T^s and in the liquid Λ_T^l

$$\Lambda_T=(1-\phi)\Lambda_T^s+\phi X^l\Lambda_T^l \tag{11}$$

where ϕ denotes porosity.

Substituting the heat flux (10) into (9) and expanding the entropy function $s(T, X^l, X^v)$ with respect to the parameters of state, we get

$$\rho^s c_v\dot{T}+\rho^s T\left(s^l\dot{X}^l+s^v\dot{X}^v\right)=\text{div}\left[\Lambda_T\text{grad}\,T\right] \tag{12}$$

where $T(\partial s/\partial T)=c_v=c^s+c^l\ X^l+c^v\ X^v$ is the total specific heat of the body and c^α is the specific heat of constituent α.

For the FDRT, where the liquid flux disappears and the vapor flux can be considered for small one, the second term in Eq. 12 can be rewritten as follows

$$\begin{aligned}\rho^s T\left(s^l\dot{X}^l+s^v\dot{X}^v\right)&=T\left(s^l\hat{\rho}^l+s^v\hat{\rho}^v\right)=-l\hat{\rho}^l=l\varpi\left(\mu^l-\mu^v\right)\\&=l\omega(c_T\vartheta+c_X\theta)\end{aligned} \tag{13}$$

where $l=T(s^v-s^l)$ is the latent heat of evaporation.

Thus, the differential Eq. 12 for determination of temperature can take the form

$$\dot{\vartheta}=D_T\nabla^2\vartheta-l\frac{\omega}{\rho^s c_v}(c_T\vartheta+c_X\theta) \tag{14}$$

where $D_T(T, X^l)=\Lambda_T(T, X^l)/\rho^s c_v$ is the thermal diffusivity.

Equations 8 and 14 constitute the complete system of equations for determination of liquid content and temperature distributions in a drying body, including the phase transitions of liquid into vapor inside the body. These equations have to be completed with the initial and boundary conditions for the purpose of their explicit solution. Such conditions are formulated in section Two-Dimensional Problem for the cylindrically shaped sample dried convectively.

Stresses and deformations

Total stress σ_{ij} in a fluid saturated porous medium consists in general of the stress in the skeleton and the stress in the pore fluid. Mostly, the stress deviator in fluid is considered as much smaller than that in the skeleton, so the fluid stress is expressed simply as the pore pressure. The equilibrium of internal forces in a fluid saturated porous body is expressed by stresses and gravity forces, that is

$$\sigma_{ij,j}+\rho g_i\approx 0 \tag{15}$$

where σ_{ij} denotes the stress tensor, ρ is the mass density of the body, g_i is the gravity acceleration (neglected in further considerations), and index $(,j)$ denotes differentiation with respect to coordinate $j=\{x,y,z\}$. The inertia forces are neglected here due to the assumption made earlier that drying processes proceed quasistatically.

The physical relation for elastic materials is convenient to split into deviatory and spherical parts, that is

$$s_{ij}=2Me_{ij},\ \ \sigma=K(\varepsilon-\varepsilon^{(TX)}) \tag{16}$$

where $s_{ij}=\sigma_{ij}-\sigma\delta_{ij}$ is the stress deviator, $\sigma=\sigma_{ij}/3$ is the spherical stress, $e_{ij}=\varepsilon_{ij}-(\varepsilon/3)\delta_{ij}$ is the strain deviator, $\varepsilon=\varepsilon_{ii}$ is the volumetric strain, and M and K are the elastic shear and bulk modules, respectively.

The temperature and moisture content involve the volumetric thermal-humid strain, which is expressed as

$$\varepsilon^{(TX)}=3\left(\kappa^{(T)}\vartheta+\kappa^{(X)}\theta\right) \tag{17}$$

where $\kappa^{(T)}$ and $\kappa^{(X)}$ are the, respective, coefficients of linear thermal and humid expansion.

Substituting the physical relations 16 into the equilibrium condition of internal forces 15, one obtains the differential equations expressed in terms of strains, temperature, and moisture content namely

$$\left[2M\varepsilon_{ij}+(A\varepsilon-\gamma_T\vartheta-\gamma_X\theta)\delta_{ij}\right]_{,j}+\rho g_i=0 \tag{18}$$

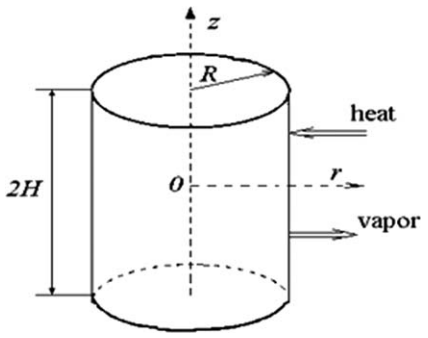

Figure 2. Cylindrical sample during convective drying.

where $A = K - 2M/3$, $\gamma_T = 3K\kappa^{(T)}$, $\gamma_X = 3K\kappa^{(X)}$, and the tensor of small strains is expressed by the derivative of displacement u_i

$$\varepsilon_{ij} = \frac{1}{2}\left(u_{i,j} + u_{j,i}\right) \tag{19}$$

Equation 18 after differentiating with respect to the coordinate j and using 19 becomes the displacement differential equation of the form

$$M\nabla^2 u_i + (M+A)u_{j,ji} - \gamma^{(T)}\vartheta_{,i} - \gamma^{(X)}\theta_{,i} + \rho g_i = 0 \tag{20}$$

where ∇^2 denotes the Laplace operator.

Equation 20 together with the differential equations describing liquid content 8 and temperature 14 supplemented with suitable initial and boundary conditions enable numerical calculations of drying kinetics and deformations of drying body, and indirectly the drying-induced stresses. This complete set of differential equations, termed mathematical drying model, will be formulated for the two-dimensional (2-D) geometry of cylindrical shape.

2-D Problem

Stresses and deformations

2-D problem of drying refers to cylindrical geometry expressed by the coordinates r, φ, z. We assume axial symmetry, that is, the distribution of each function (moisture content, temperature, displacement, strain, stress) is the same in all cross-sections which pass through the cylinder axis. Thus, all quantities are functions of two co-ordinates r and z. The derivatives with respect to φ disappear. This 2-D geometry sufficiently describes the thermo-hygro-mechanical state of real 3-D lump. The cylinder shown in Figure 2 will be the objective of our further considerations.[31,32]

The state of strain in the cylinder is described by radial and longitudinal displacements u_r and u_z, which read

$$\varepsilon_{rr} = \frac{\partial u_r}{\partial r}, \quad \varepsilon_{\varphi\varphi} = \frac{u_r}{r}, \quad \varepsilon_{zz} = \frac{\partial u_z}{\partial z}, \quad \varepsilon = \frac{\partial u_r}{\partial r} + \frac{u_r}{r} + \frac{\partial u_z}{\partial z} \tag{21}$$

Equations 20 expressed in cylindrical coordinates ($i = \{r,z\}$) are of the form

$$M\nabla^2 u_r + \frac{\partial}{\partial r}\left[(M+A)\varepsilon - \gamma_T\vartheta - \gamma_X\theta\right] = M\frac{u_r}{r^2} \tag{22}$$

$$M\nabla^2 u_z + \frac{\partial}{\partial z}\left[(M+A)\varepsilon - \gamma_T\vartheta - \gamma_X\theta\right] = 0 \tag{23}$$

where ∇^2 denotes the Laplace operator in cylindrical coordinates, that is

$$\nabla^2 = \frac{\partial^2}{\partial r^2} + \frac{1}{r}\frac{\partial}{\partial r} + \frac{\partial^2}{\partial z^2} \tag{24}$$

The gravity forces are neglected in Eqs. 22 and 23 due to the previous assumption that they are small in samples of small dimension, as it is in the cylinder presented in Figure 2.

Deformations and stresses in dried bodies arise as a result of moisture removal and heating or cooling of the body. There are no external mechanical forces acting on the sample surface during drying, so we assume zero-valued radial and longitudinal stresses on these surfaces, that is

$$\sigma_{rr}|_{r=R} = \left[2M\frac{\partial u_r}{\partial r} + A\varepsilon - \gamma_T\vartheta - \gamma_X\theta\right]|_{r=R} = 0 \tag{25a}$$

$$\sigma_{zz}|_{z=H} = \left[2M\frac{\partial u_z}{\partial z} + A\varepsilon - \gamma_T\vartheta - \gamma_X\theta\right]|_{z=H} = 0 \tag{25b}$$

The other two boundary conditions assume zero-valued radial and longitudinal displacements at the cylinder axis and in the center of the cylinder, that is

$$u_r|_{r=0} = 0 \text{ and } u_z|_{z=0} = 0 \tag{25c}$$

The circumferential stress for elastic cylinder reads

$$\sigma_{\varphi\varphi} = 2M\frac{u_r}{r} + A\varepsilon - \gamma_T\vartheta - \gamma_X\theta \tag{26}$$

The shear stresses for elastic cylinder are expressed as

$$\sigma_{rz} = M\left(\frac{\partial u_r}{\partial z} + \frac{\partial u_z}{\partial r}\right) \tag{27}$$

Shear modulus M and bulk modulus A can be expressed by Young's modulus E and Poisson's ratio v as follows

$$M = \frac{E}{2(1+v)}, \quad A = \frac{Ev}{(1-2v)(1+v)}, \quad 3K = 2M + 3A \tag{28}$$

Poisson's ratio is assumed to be constant and equal to $v = 0.4$. Young's modulus on the other hand is assumed to be a function of moisture content, as presented in Figure 3.

It was stated[33,34] that kaolin-clay shrinks in the moisture range from 0.4 to 0.2 (dry basis). Below the limit 0.2, the shrinkage is insignificant. To take this fact into account, the coefficient denoted by $\gamma_X = 3K\kappa^{(X)}$ is assumed to be moisture dependent, as is presented Figure 4.

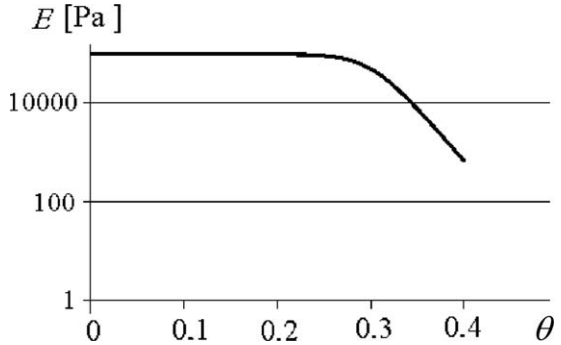

Figure 3. Young's modulus as a function of moisture content.

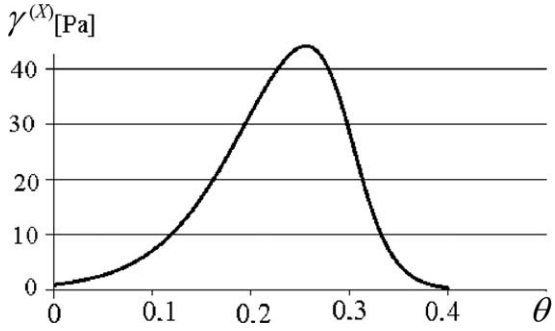

Figure 4. Dependence of coefficient $\gamma_X = 3K\kappa^{(X)}$ on moisture content.

Figure 4 includes two opposed phenomena, namely, that the shrinkage decreases and the Young modulus increases with the decrease of moisture content, and inversely.

The state of stress in the cylinder is fully described by the following components of the stress tensor: σ_{rr}, $\sigma_{\varphi\varphi}$, σ_{zz}, σ_{rz}. The overall effective stress is defined on the basis of the Huber-von Mises–Hencky energy hypothesis, namely

$$\sigma_{\text{eff}} = \frac{1}{2}\sqrt{(\sigma_{rr}-\sigma_{zz})^2+(\sigma_{rr}-\sigma_{\varphi\varphi})^2+(\sigma_{\varphi\varphi}-\sigma_{zz})^2+6\sigma_{rz}^2} \quad (29)$$

The material failure can take place if the effective stress exceeds the admissible one, which expresses the yield stress or the strength of the material at given moisture content. The admissible stress was determined experimentally by Musielak[33] for kaolin clay at different moisture contents. The experimental data for admissible stress have been interpolated by the following function

$$\sigma_{\text{adm}} = \sigma_0 + \sigma_X \exp(-C_\sigma \theta) \quad (30)$$

where $\sigma_0 = 9153$ Pa, $\sigma_X = 7307$ Pa, and $C_\sigma = 7$.

Figure 5 presents the graphical dependence of admissible stresses on moisture content according to formula (30).

The failure of the material may happen in those regions of the dried kaolin-clay cylinder where the material strength is violated, that is, when

$$\sigma_{\text{eff}} \geq \sigma_{\text{adm}} \quad (31)$$

As seen from the formulas 25,a,b, 26, and 27, the stresses are dependent on temperature and moisture content. These functions are determined in the section to follow.

Drying kinetics

Distribution and time evolution of liquid content and temperature will be determined for both the CDRP and the

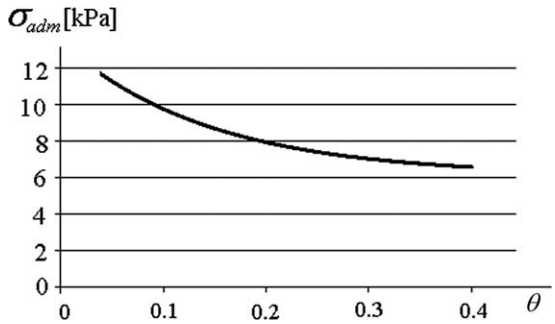

Figure 5. Alteration of material strength with variable moisture content.

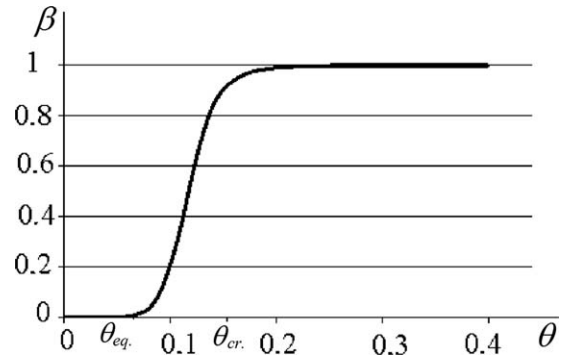

Figure 6. Coefficients of the convective vapor exchange β as a function of liquid content

FDRP. Differential Eqs. 8 and 14 in cylindrical geometry take the form

$$\rho^s \dot{\theta} = \Lambda^l \left(\frac{\partial^2}{\partial r^2}+\frac{1}{r}\frac{\partial}{\partial r}+\frac{\partial^2}{\partial z^2}\right)(c_T\vartheta + c_X\theta) - \omega(c_T\vartheta + c_X\theta) \quad (32)$$

$$\dot{\vartheta} = D_T\left(\frac{\partial^2\vartheta}{\partial r^2}+\frac{1}{r}\frac{\partial\vartheta}{\partial r}+\frac{\partial^2\vartheta}{\partial z^2}\right) - l\frac{\omega}{\rho^s c_v}(c_T\vartheta + c_X\theta) \quad (33)$$

The boundary and initial conditions for moisture and heat transfer are as follows

$$\text{grad}\,\theta\Big|_{\substack{r=0\\z=0}} = 0, \; -\Lambda^l \text{grad}\,(c_T\vartheta + c_X\theta)|_B \cdot \boldsymbol{n} = \alpha_m(\theta)\left(\mu^v|_B - \mu_a^v\right) \quad (34a)$$

$$\text{grad}\,\theta\Big|_{\substack{r=0\\z=0}} = 0, \; \Lambda_T \text{grad}\,\vartheta|_{\partial B} \cdot \boldsymbol{n} = \alpha_T(\vartheta|_B - \vartheta_a) - l\alpha_m(\theta)\left(\mu^v|_B - \mu_a^v\right) \quad (34b)$$

$$\theta(r,z,t)|_{t=0} = \theta_0 = \text{const}, \quad \vartheta(r,z,t)|_{t=0} = \vartheta_0 = \text{const} \quad (35)$$

where $\mu^v|_B$ and μ_a^v denote the chemical potentials of vapor at the boundary surface and in the ambient air, α_m and α_T are the coefficients of the convective vapor and heat exchange between the dried body and the ambient air, and θ_0 and ϑ_0 are the initial moisture content and temperature, respectively.

The conditions on the left hand side of 34a and 35b express the symmetry in distribution of moisture content and temperature with respect to the cylinder centre, while those on the right hand side express the convective mass and heat transfer between the cylinder boundary surface and the ambient air.

The coefficients of the convective vapor exchange $\alpha_m(\theta)$ is a function of liquid content in the drying body and is expressed in the form

$$\frac{\alpha_m(\theta)}{\alpha_{m0}} = \begin{cases} 1 & d\text{la } \theta \geq \theta_{\text{cr}} \\ \beta(\theta) & d\text{la } \theta_{\text{eq}} \leq \theta \leq \theta_{cr} \\ 0 & d\text{la } \theta \leq \theta_{\text{eq}} \end{cases} \quad (36)$$

Figure 6 presents the graphical shape of the convective vapor exchange coefficient as a function of liquid content in drying body.

The graph in Figure 6 suggests that the convective exchange of moisture is maximum in the first stage of drying, say during CDRP, and then this exchange decreases gradually and stops when the moisture content reaches equilibrium with ambient air.

The chemical potentials of vapor at the boundary surface and in the ambient can be written in the following form[35]

$$\mu^v|_B(p,T|_B,x|_B)=\mu^v(p,T|_B)+\Re T|_B\ln x|_B \quad (37a)$$

$$\mu_a^v(p,T_a,x_a)=\mu^v(p,T_a)+\Re T_a\ln x_a \quad (37b)$$

where p is the air total pressure, $\Re$ is the gas constant, $T|_B$ and T_a are the temperatures, and $x|_B$ and x_a the mole fractions of vapor at the boundary surface and in the ambient air, respectively.

In convective drying, the temperatures at the boundary surface and in the ambient air do not differ much from each other (say max 20 to 30°C), so that the thermo-diffusional flux of vapor can be neglected, and we may write[36]

$$\mu|_B-\mu_a=\mu^v(p,T|_B)-\mu^v(p,T_a)+\Re(T|_B\ln x|_B-T_a\ln x_a)\approx \Re T_a\ln\frac{x|_B}{x_a} \quad (38)$$

The driving force of convective vapor transfer is convenient to write using the relative air humidity $\varphi=(p_w/p_{\mathrm{wn}})_T$ and the vapor partial pressure for the saturated state p_{wn}, that is

$$\ln\frac{x|_B}{x_a}=\ln\frac{p_w|_B}{p_{\mathrm{wa}}}=\ln\frac{\varphi|_B p_{\mathrm{wn}}(T|_B)}{\varphi_a p_{\mathrm{wn}}(T_a)} \quad (39)$$

The air relative humidity close to the surface of drying body $\varphi|_B$ depends on the sample moisture content. We assume the following form of the air relative humidity at the sample surface[28]

$$\varphi|_B=\begin{cases}1 & \text{for } X|_B\geq X_{cr}\\ 1-(1-\varphi_a)\dfrac{X_{cr}-X|_B}{X_{cr}-X_{eq}} & \text{for } X_{cr}\geq X|_B\geq X_{eq}\end{cases} \quad (40)$$

In the above equations, φ_a and T_a (K) or ϑ_a (°C) denote the relative humidity and the temperature of air, termed further as the parameters of drying, and X_{cr} and X_{eq} are the critical and the equilibrium moisture contents in dried sample (parameters determined experimentally). Function $p_{\mathrm{wn}}(T)$ is given in the literature in the form of tables.[5]

Drying Control

Prediction of material damage

The numerical calculations of drying kinetics and stresses were performed for the cylindrical sample made of kaolin. The system of differential equations presented above was solved with the finite element method applied to spatial derivatives, and the discretization of time derivative was made with the three step method of finite differences.

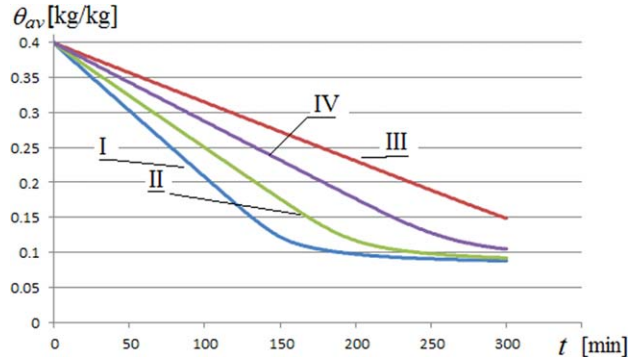

Figure 7. Drying curves for different drying parameters appointed in Table 1.

[Color figure can be viewed in the online issue, which is available at wileyonlinelibrary.com.]

Table 1. Drying Parameters and Results of Four Different Processes

Process Number	Air Temperature ϑ_a (°C)	Air relative Humidity, ϕ_a (%)	Time of Drying until $\theta_{av}=0.1$, t (min)	Effective Stress σ_{eff} (kPa)
I	90	20	189	10.58
II	80	20	240	10.37
III	70	40	350	5.43
IV	70	10	315	6.49

The following data were applied for numerical calculations[4]

$H=40$ mm $\quad R=40$ mm

$\Lambda_T^s=1.78W\cdot m^{-1}\cdot K^{-1}$ $\quad \Lambda_T^l=1.597W\cdot m^{-1}\cdot K^{-1}$

$c_T=3.6\,\mathrm{m^2s^{-2}K^{-1}}$ $\quad c_X=10^{-3}\mathrm{m^2\cdot s^{-2}}$

$f_0=6\times10^{-7}\,\mathrm{kg\,s^2m^{-5}}$ $\quad \omega_0=2.5\times10^{-6}\mathrm{kg\cdot sm^{-5}}$

$c^s=728.5\,\mathrm{J\cdot kg^{-1}K^{-1}}$ $\quad c^l=4186\mathrm{J\cdot kg^{-1}K^{-1}}$

$\alpha_m=8.64\cdot10^{-5}\mathrm{kg\,sm^{-4}}$ $\quad \alpha_T=150\mathrm{W\cdot m^{-2}K^{-1}}$

$\rho^s=1600\,\mathrm{kg\,m^{-3}}$ $\quad \Re_0=461\mathrm{J\cdot kg^{-3}\cdot K^{-1}}$

$l=2000\,\mathrm{kJ\,kg^{-1}}$ $\quad \phi=0.5$

The intensity of stress generation in materials during drying depends on the drying rate. Higher drying rate causes greater nonuniformity in moisture distribution and nonuniform shrinkage, which is the reason for stress generation.

Figure 7 presents the curves of drying for four drying processes according to the drying parameters appointed in Table 1.

Analysis of the results given in Table 1 and the drying curves presented in Figure 7 allows to state that the highest drying rate corresponds to process I and the lowest one to process III. Unfortunately, the high drying rate causes a nonuniform moisture distribution and has an effect on nonuniform shrinkage and thus on stress generation. As it is given in Table 1, the greatest effective stress corresponds to the highest drying rate and the smallest stress to the lowest

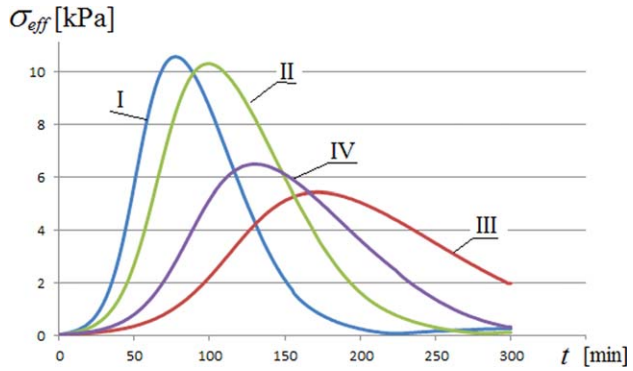

Figure 8. Time evolution of maximal effective stresses corresponding to the four drying processes (Table 1)

[Color figure can be viewed in the online issue, which is available at wileyonlinelibrary.com.]

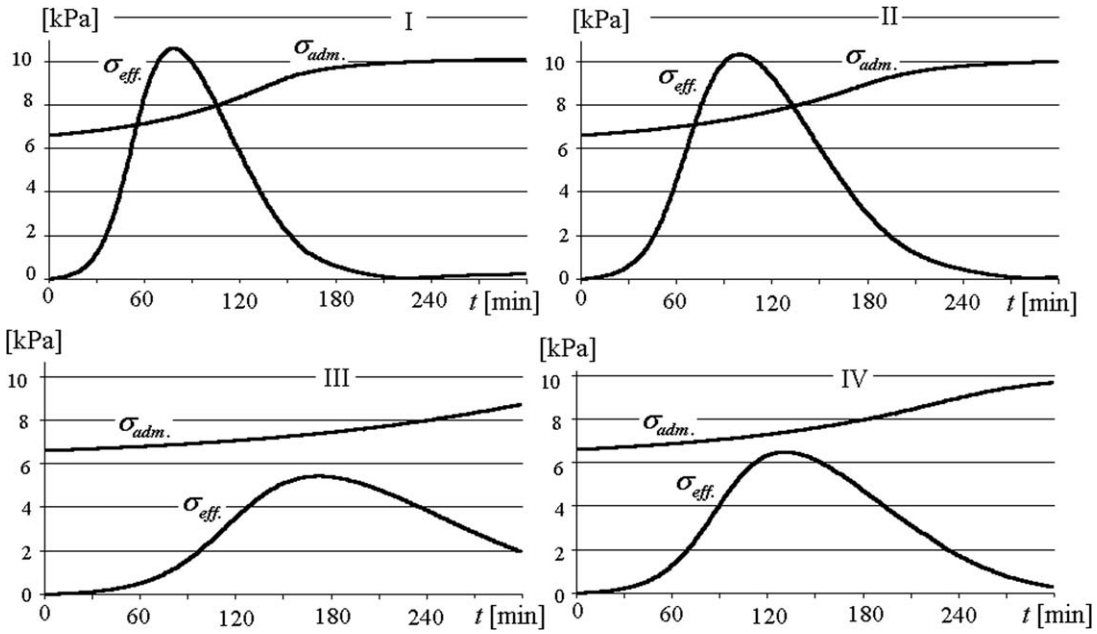

Figure 9. Time evolution of the effective and the admissible stresses corresponding to the four drying processes at point (*R*,*H*) of dried cylinder.

drying rate. So, by intensive drying, the material damage is highly probable.

Figure 8 presents the time evolution of maximal effective stresses in point ($r = R$, $z = H$) of the cylinder corresponding to the four drying processes appointed in Table 1 and drying curves presented in Figure 7.

The essential information about the possible damage of material during drying with different drying rates follows from comparison of the plots presenting the time evolution of the effective stress and the admissible stress simultaneously, which expresses the strength of dried material. Figure 9 presents the courses of the effective stress and the admissible stress in point (*R*,*H*) of the cylinder for the four processes appointed in Table 1.

It is obvious that the material strength of drying body is evidently a function of moisture content, so it has to change during drying. As it follows from the graphs presented in Figure 9, in two cases, namely in processes I and II, the effective stress was greater at some time than the admissible stress. The moments when the effective stress is greater than the admissible one can be just the moments of material damage.

The graphs corresponding to processes III and IV reveal some reserve of material strength with respect to the maximal effective stress. The material strength reserve informs us that there is a possibility to accelerate the drying rate to some extent. However, because of nonlinear mechanical behavior of the material during drying, it is difficult to foresee how the stresses will be changed after the modification of drying parameters. Therefore, to arrange a possibly high rate of drying process, in which the material will not experience damage, it is necessary to carry out a number of numerical experiments called the optimization procedure.

Optimal Process by Stable Drying Conditions

The goal of this section is to find the optimal value of temperature ϑ_a for a given absolute humidity Y_a of the drying medium (usually air) at which the drying rate will be maximal and the drying material will not suffer damage. The material is assumed to be elastic.

The problem was analyzed for four different values of absolute air humidity Y_a (Table 2). The algorithm of finding optimal temperature ϑ_a for a given humidity Y_a was as follows: the air was assumed to have the initial temperature $\vartheta_a = 70°C$ in each tested process. The procedure of finding optimal temperature consisted of 20 steps. If during the simulated process the effective stress exceeded the admissible one, which meant material damage, the calculations were broken. The program automatically diminished the drying air temperature and sequential calculations began in the next step. If in the next calculations, the final moisture content $\theta_{eq} = 0.1$ was reached without exceeding the admissible stress by the effective one, next calculations were realized with increased temperature of the drying medium. In the subsequent calculations, the temperature of the drying medium was corrected with a more and more smaller value. For the optimal temperature, ϑ_a was considered as one at which the sample reached the equilibrium moisture content $\theta_{eq} = 0.1$ in the shortest time and without material damage, that is, the effective stress was close to the admissible one but not exceeding it. The optimal temperatures ϑ_a for a given humidity Y_a are presented in Table 2.

Table 2. Optimal Temperatures of Drying Medium for a Given Humidity (Elastic Material)

Process Number	Air Absolute Humidity, Y_a (−)	Beginning Temperature, ϑ_a (°C)	Optimal Temperature, ϑ_a (°C)	Time of Drying Until $\theta_{av} = 0.1$, t (min)
1	0.0099	70	62.90	364.5
2	0.02476	70	71.02	326.0
3	0.02977	70	72.70	316.5
4	0.07736	70	84.00	274.5

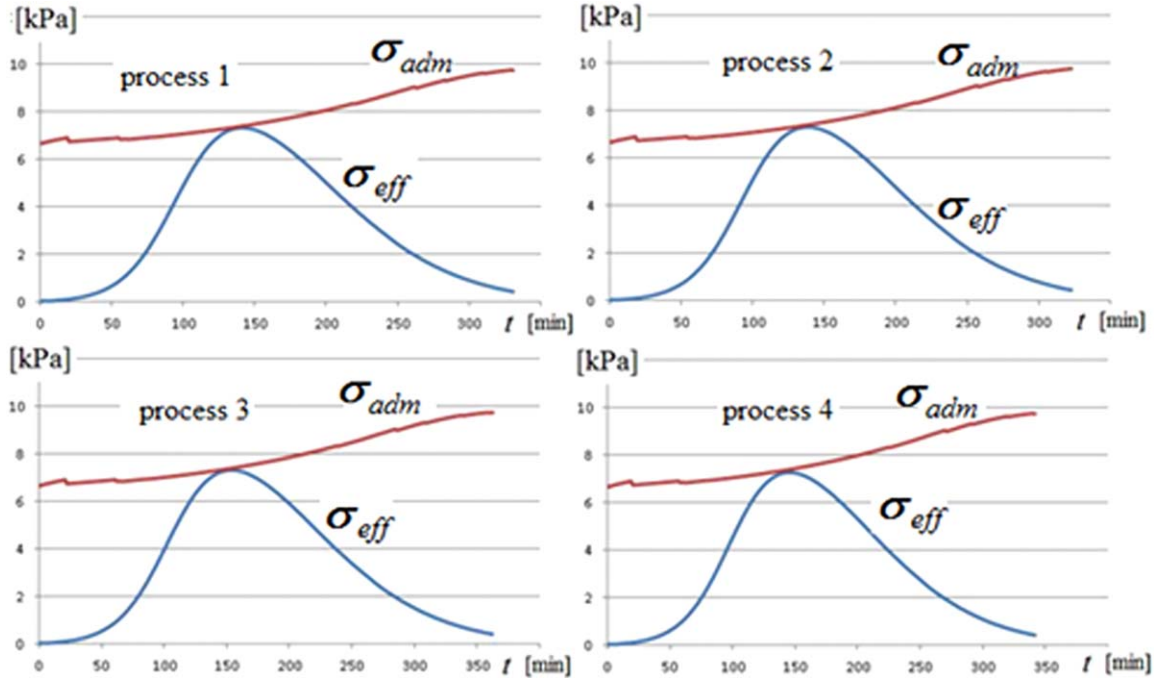

Figure 10. Courses of the maximal effective stresses σ_{max} and the admissible stresses σ_{adm} in point (*R,H*) of the cylindrical sample for drying parameters presented in Table 2.

[Color figure can be viewed in the online issue, which is available at wileyonlinelibrary.com.]

Figure 10 shows the course of maximal effective stresses and the admissible stresses during the simulated optimal drying with parameters described in Table 2.

Figure 10 illustrates the change of admissible stresses expressing material strength during drying, and we see that the material strength reveals a continuous increase in the course of drying. The effective stress on the other hand gains its maximum at some moment of drying time and then tends to zero. The effective stress was calculated in the edge (*R*,*H*) of the cylindrical sample, where it reaches maximal value. As seen from Figure 10, the optimal drying process was run in such a way that the maximal stress touched but never exceeded the strength of the material, so the dried sample was not damaged. Simultaneously, all the optimal processes were carried out with possibly maximum drying rate for the given humidity and optimal temperature presented in Table 2.

Effective drying process

An exact control of drying parameters is difficult to carry out not only because of problems with precise parameter setting but also because of inertia effects both in the drying system and the measuring instruments. The instruments can properly measure drying parameters such as temperature and air humidity only in immobile drying medium. In movable medium, the measurement of these parameters is less reliable and has a pure theoretical meaning. Some solution to get results having practical meaning is to formulate an optimization problem based on numerical simulations which is helpful in finding an optimal drying process. Such a problem is considered and discussed below.

Let us consider the problem of convective drying of a kaolin-clay cylinder in a chamber dryer and find optimal process through the controlled work of the dryer, namely, through acceleration of the drying medium (air) exchange with the surrounding by switching the fan on and off, and through change of the medium temperature by switching the heater on and off during drying (Figure 11).

An optimal operation of the fan F and heater H in the dryer presented in Figure 11 was realized through the genetic algorithm method. The temporary values of T_a and Y_a are substituted into boundary conditions 34a,b. using the relation $Y_a = \varphi_a p_{wn}/(p - \varphi_a p_{wn})$ Two-hour operation of the dryer is described by the sequence of 120 pairs of 0 and 1.

The drying effectiveness is assessed by the evaluation of such quantities as the time of drying, the quality of dried product, and the energy consumption. The time of drying is estimated on the basis of drying curves (see Figure 7 and Table 1). The quality of a dried product is regarded as good if the effective stress does not overcome the admissible one at each point of the product (see Figure 10). Thus, we look for the process offering low consumption of energy at good quality of dried product and possibly short drying time.

To find such an optimal drying process via numerical simulations in this article, we have divided the procedure into three stages. In the first stage lasting 25 min, both the fan and the heater have worked together to ensure maximum drying rate. In the second stage of 180 min, the operation of the fan and the heater was controlled. At the end of the second stage, one expects the moisture content in a drying body to be low enough, at which the stresses generated by nonuniform distribution of moisture are small and cannot cause material damage. So, in the third stage of drying, the fan and the heater should be switched on again to maximize the drying rate. The third stage is continued until the moisture content reaches the equilibrium value with the surroundings, here it is assumed to be $X_{eq} = 0.1$.

Thus, to minimize the total energy consumption, the drying process should be arranged in such a way as to minimize the duration of the third drying stage, in which the fan and

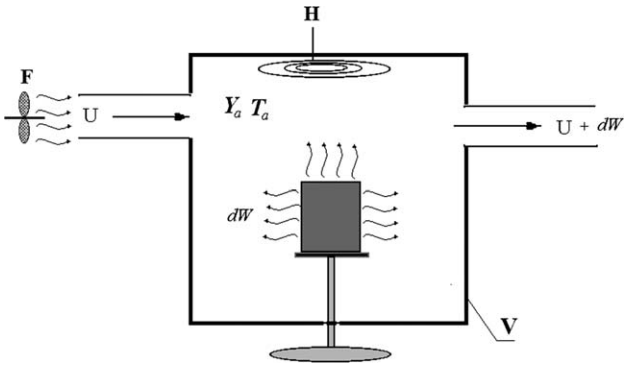

Figure 11. Scheme of the chamber dryer with controlled temperature and air blow.

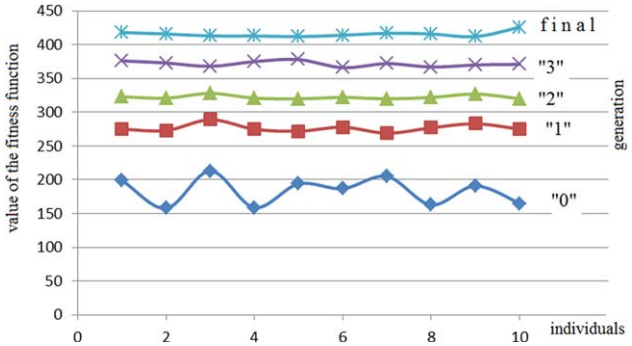

Figure 12. Action of the genetic algorithm.

[Color figure can be viewed in the online issue, which is available at wileyonlinelibrary.com.]

the heater, that is, the big energy consumers work together. It is possible to shorten the third drying stage through better control of the process in the second stage of drying. By the energy calculations, a difference in energy usage by the heater and by the fan was taken into account, namely, it was assumed that the power of heater is five times greater than that of the fan. The optimizing program computes consumption of energy and counts that every minute the energy consumption increases five times if the heater is used, and once when the fan is used. The objective function E, termed the aim function, expresses the profit from optimal drying, that is, it should take maximum for a given process. It was assumed that possible profit for a given process is equal to $E_r = 700$ units minus the costs of energy consumption E_c. So

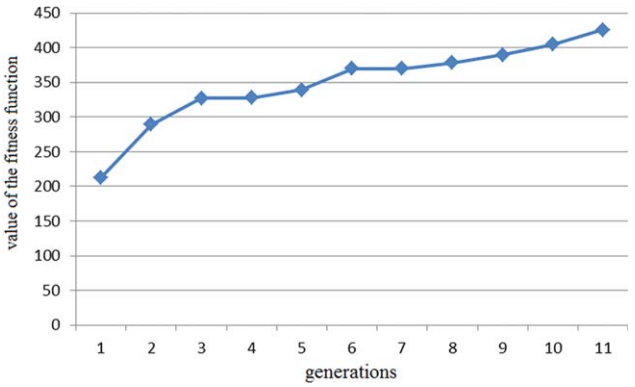

Figure 13. The fitness of the best elements for the effective process.

[Color figure can be viewed in the online issue, which is available at wileyonlinelibrary.com.]

the aim function $E = E_r - E_c$ will reach maximum when the energy consumption will be minimal.

The problem was solved based on the mechanistic model of drying for the kaolin clay considered as elastic material.

Figure 12 illustrates the action of the optimization procedure with respect to the minimum energy consumption.

One can observe in this figure how the adjustment function has grown for the subsequent elements obtained with the use of the genetic algorithm.

As it was mentioned in the Introduction, the action of the genetic algorithm consists of multiple repetitions of the following actions: estimation of adjustment, selection, crossbreeding, mutation, and modification of initial population. Next, the genetic algorithm comes back to the "selection" point and repeats the procedure again to finally get a satisfactory result.

Figure 13 illustrates the selection of the best elements, which are the most profitable for the effective process (minimum of energy consumption).

The initial element of the adjustment function in Figure 13 was constructed through the casting method, and the next were created through multiple repetition of the genetic algorithm.

Figure 14 presents the results of optimization using the genetic algorithm method.

As seen from the plot in Figure 14a, the drying curve for the optimal drying process is not as simple as it is by

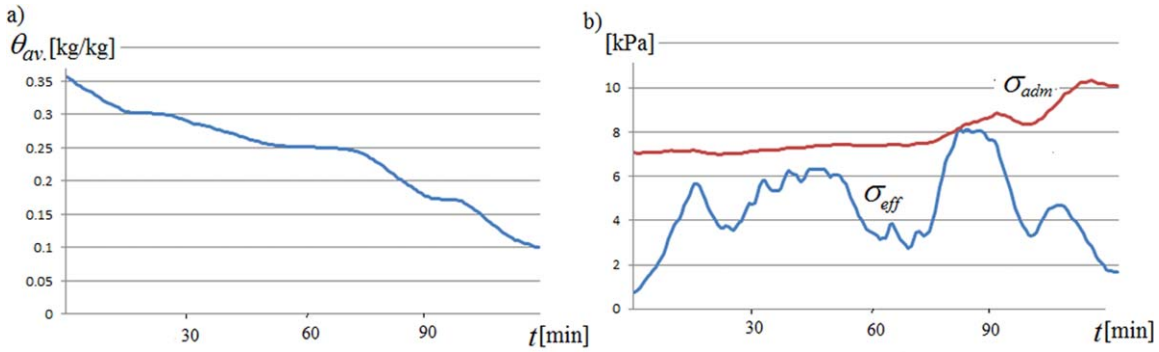

Figure 14. Optimal process: (a) optimal drying curve, (b) time evolution of the effective and the admissible stresses corresponding to optimal process.

[Color figure can be viewed in the online issue, which is available at wileyonlinelibrary.com.]

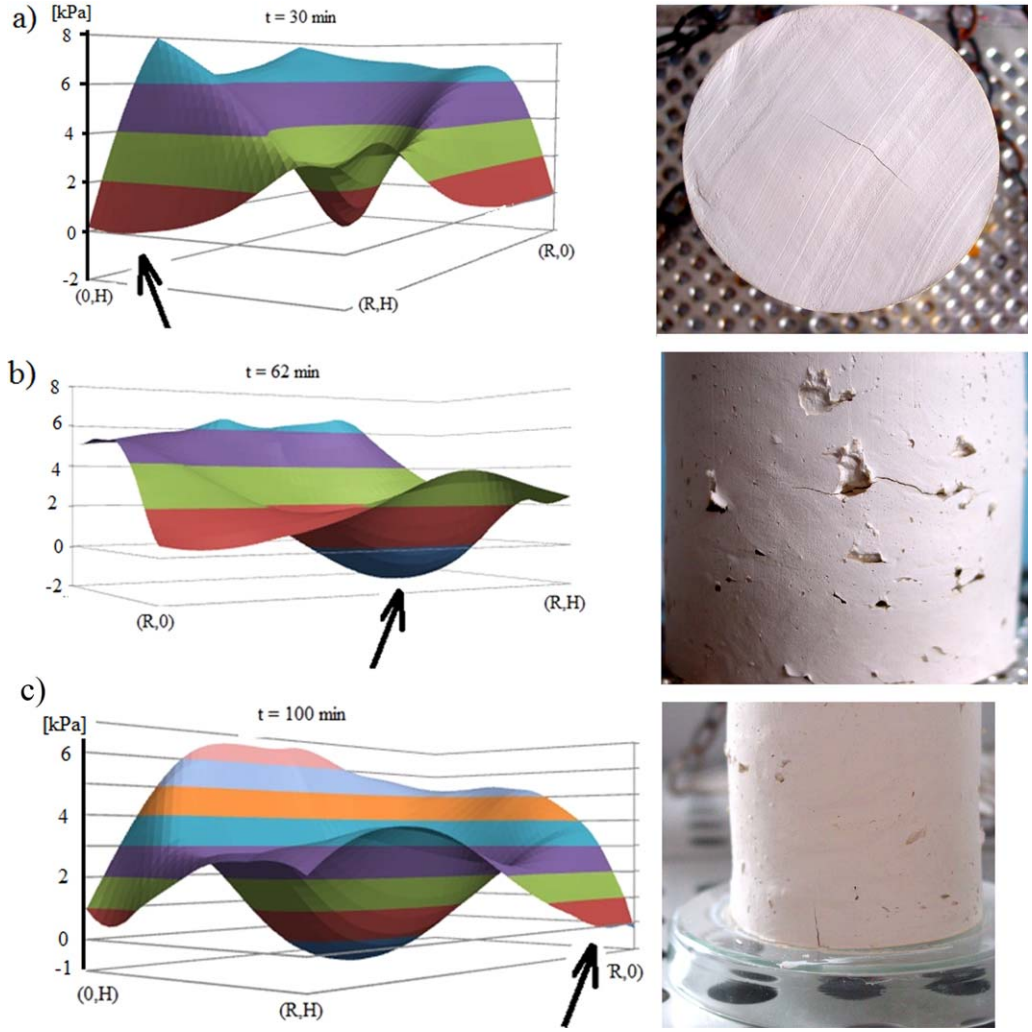

Figure 15. Illustration of material damage during convective drying.

[Color figure can be viewed in the online issue, which is available at wileyonlinelibrary.com.]

conventional drying with constant drying condition.[4] This drying curve suggests that the optimized process required periodical acceleration and a slowdown of the drying rate, which is manifested by the waving drying curve. Only in such a way, is it possible to prevent the drying material from damage, as proved by the plots of effective and admissible stresses presented in Figure 14b. The effective stress presented in this figure never overcomes the admissible stress, which means that in such a process the material does not suffer damage.

In conclusion, one can say that the effective drying process ensures a reasonable drying time at possibly low-energy consumption, and more importantly, preserves a good quality of dried product, that is, the strength of dried material is not violated as revealed the plots in Figure 14b.

Model Validation

The computer-simulated convective drying of cylindrical kaolin-clay samples and the method of optimal control of such processes through suitable choice of the drying medium (air) parameters were presented above. On the basis of the stress analysis in drying body, the spots of possible material damage caused by intensive drying were predicted. The program of changes of drying parameter at intensive drying was elaborated on the observation of the mechanical effects caused by such drying, whose results are presented in Figure 15.

Having in mind the optimization procedure of drying processes discussed above, we conclude that each optimal process should possibly begin with intensive drying. At the moment when the effective stresses approach the admissible ones, the parameters of drying air should be modified in such a way as to slow down the intensity of drying. If the intensive drying is not slowed down, the damage of the drying sample is highly realistic, which shows the photographs on the right hand side of Figure 15. The pictures on the left hand side of Figure 15 presents the distribution of function being the difference between admissible and effective stress ($\sigma_{\mathrm{adm}} - \sigma_{\mathrm{eff}}$).

On the upper right photograph (Figure 15a), the upper surface of the kaolin-clay cylinder experiences cracks, which appears after 30 min drying. In point (0, H), the radial stresses σ_{rr} reach maximum at this time, that is, at early stage of drying.

After 60 min of intensive drying, it is possible for another crack to occur on the external surface in the middle of the cylinder (Figure 15b). At this time, the effective stresses

attain the maximum value inside the cylinder, and the greatest share in the effective stress has the shear stress σ_{rz}. In such a case, the damage may occur inside the cylinder (not visible from outside) or may cause crack on the external surface of the cylinder, even along the whole circumference of the cylinder.

The third picture (Figure 15c) was obtained when the drying process followed the prescribed optimal program up to 90 min of drying, and after this time the process was carried out with maximum intensity. In such a case, the damages may arise, similarly as in the previous case, that is, in the cylinder's interior as a result of big shear stresses σ_{rz}, and at the bottom of the cylinder in point $(R,0)$ as a result of big circumferential stresses $\sigma_{\varphi\varphi}$ (Figure 15c).

Conclusions

The high drying rate has a negative influence on product quality, which is proved in Figure 9 (processes I and II). The high drying rate caused violation of the material's strength, which is evidenced by the fact that the effective stresses exceeded the admissible ones. In processes III and IV, on the other hand, the effective stresses are far from the admissible ones, which mean that in this case the drying rate was too low. Thus, one has to look for optimal drying parameters, which allow fast drying without violation of material strength. Such optimal processes are presented in Figure 10. In these processes, the drying rate is possibly high but the effective stresses never exceeded the admissible once, although they are close to each other as much as possible.

Based on the numerically simulated drying tests presented above, one can state that the drying regime can be a severe one at the beginning to involve a high drying rate. At the moment when the effective stresses approach the admissible ones, the drying conditions should be modified to slow down the drying rate and to avoid damage of the dried sample. Briefly speaking, the effective drying process needs continuous control. Optimization of drying processes with respect to minimum economic costs and/or minimum drying time should take into account the mechanical state of a dried material to protect it against destruction and bad final quality. The drying rates are allowed to be accelerated when the drying induced stresses are small, and slowed down when the stresses tend to overcome the strength of the material. Such rigorous principles of rational control of drying are not generally known, so there is a need for the formulation of mathematical optimization procedure to find optimal processes followed by their experimental validation.

Acknowledgment

This work was carried out as a part of the research project N N209 031 638 sponsored by Ministry of Science and High Education.

Notation

A = elastic bulk modulus, MPa
c_v = specific heat, J/kg K
c_T = coefficient of thermodiffusion, m^2/s^2 K
c_X = coefficient of diffusion, m^2/s^2
D_T = thermal diffusivity, m^2/s
e_{ij} = strain deviator, 1
$f(X^l)$ = parameter dependent on pore structure and liquid content, kg s^2/m^5
g_i = gravity acceleration, m/s^2
H = cylinder height, m
l = latent heat of evaporation, J/kg
K = elastic volumetric modulus, MPa
M = elastic shear modulus, MPa
p = pressure, Pa
$\boldsymbol{q}$ = heat flux, W/m^2
r, R = cylinder radius, m
$\Re$ = individual gas constant, J/kg K
s, s^α = entropy, entropy of α-constituent, J/kg K
s_{ij} = stress deviator, Pa
t = time, s
T = temperature, K
$\boldsymbol{u}(u_r, u_z)$ = displacement vector, m
$\boldsymbol{W}^\alpha$ = mass flux of α-constituent, kg/m^2 s
x_a, x_n = mole fractions of vapor in air, 1
x, y, z = spatial Cartesian coordinates, m
X^α = dry basis content of α-constituent, 1
Y = absolute air humidity, kg H_2O/kg dry air

Greek letters

α_m = coefficient of convective vapor exchange, kg s/m^4
α_T = coefficient of convective heat exchange, W/m^2 K
ϕ = porosity, 1
φ = air relative humidity, 1
κ = coefficient of phase transition efficiency, 1
$\kappa^{(T)}$ = coefficient of thermal expansion, 1/K
$\kappa^{(X)}$ = coefficient of humid expansion, 1
ε_{ij} = strain tensor, 1
ε = volumetric strain, 1
σ_{ij} = stress tensor, Pa
σ = spherical stress, Pa, surface tension, N/m
ρ, ρ^α = mass density, mass concentration of α-constituent, kg/m^3
$\hat{\rho}^\alpha$ = rate of α-constituent mass change by phase transitions, kg/m^3 s
μ^α = chemical potential of α-constituent, J/kg
ν = Poisson's ratio, 1
η = viscosity, Pa s
ω = phase transition intensity, kg s/m^5
$\vartheta = T - T_r$ = temperature difference, K or °C
$\theta = X^l - X^l_r$ = moisture content difference, 1
$\Lambda^l(T,X^l)$ = liquid mobility coefficient, kg s/m^4
Λ_T = coefficient of thermal conductivity, W/m·K

Subscripts

a = ambient air
av = average
m = moisture
adm = admissible
eff = effective
cr = critical
eq = equilibrium
v = volume
T = thermal
w = water
wn = water saturated

Superscripts

l = liquid
s = solid
$\boldsymbol{v}$ = vapor

Literature Cited

1. Garcia H, Bueno JL. Improving energy efficiency in combined microwave-convective drying. *Drying Technol*. 1998;16:123–140.
2. Dufour P. Control engineering in drying technology: review and trends. *Drying Technol*. 2006;24(7):889–904.
3. Kowalski SJ. Control of mechanical processes in drying. *Theory and experiment. Chem. Eng. Sci*. 2010;65:890–899.
4. Rybicki A. *Control of Drying Processes of Materials Sensitive to Shrinkage Damage. Computer Simulation*, Poznań University of Technology, Poznań Transactions No. 482, 2012 (in Polish).
5. Kudra T, Strumiłło Cz. *Drying: Principles, Applications and Design*. New York: Gordon & Breach Science Publishers, 1986.
6. Kowalski SJ, Pawłowski A. Intermittent drying: energy expenditure and product quality. *Chem Eng Technol*. 2011;34(7):1123–1129.

7. Kowalski SJ, Rajewska K, Rybicki A. Destruction of wet materials by drying. *Chem Eng Sci*. 2000;55(23):5755–5762.
8. Kowalski SJ. Thermomechanical approach to shrinking and cracking phenomena in drying. *Drying Technol*. 2001;19(5):731–765.
9. Augier F, Coumans WJ, Hugget A, Kaasschieter EF. On the risk of cracking in clay drying. *Chem Eng J*. 2002;86:133–138.
10. Banaszak J, Kowalski SJ. Theoretical and experimental analysis of stresses and fractures in clay like materials during drying. *Chem Eng Process*. 2005;44:495–503.
11. Mezheriher M, Levy A, Borde I. Heat and mass transfer and breakage of particles in drying processes. *Drying Technol*. 2009;27(7–8); 870–877.
12. Kowalski SJ, Banaszak J, Rybicki A. Damage analysis of microwave-dried materials. *AIChE J*. 2012;58(7):2097–2104.
13. Kowalski SJ, Kulczyński K. Reduction of fractures in dried clay-like materials due to specific surfactants. *Chem Eng Res Des*. 2013;91: 254–263.
14. Kowalski SJ. *Thermomechanics of Drying Processes*. Heilderberg-Berlin: Springer Verlag, 2003.
15. Michalewicz Z. *Genetic Algorithms, Data Structures, Evolution Programs*. Berlin, Springer-Verlag, 1996.
16. Scherer GW. Theory of drying, *J Am Ceram Soc*. 1986;73(1):3–14.
17. Joamaa W, Puiggali JR. Drying of shrinking materials: modeling with shrinkage velocity. *Drying Technol*. 1991;9(5):1271–1293.
18. Zhang D, Mujumdar AS. Deformation and stress analysis of porous capillary bodies during intermittent volumetric thermal drying. *Drying Technol*. 1992;10(2):421–443.
19. Hasatani M, Itaya Y. Drying-induced strain and stress: a review. *Drying Technol*. 1996;14 (5):1011–1040.
20. Banaszak J, Kowalski SJ. Drying induced stresses estimated on the base of elastic and viscoelastic models, *Chem Eng J*. 2002;86:139–143.
21. Katekawa ME, Silva MA. A review of drying models including shrinkage effects. *Drying Technol*. 2006;24(1):5–20.
22. Itaya Y, Uchiyama S, Mori S. Internal heating effect and enhancement of drying of ceramics by microwave heating with dynamic control. In: Kowalski SJ, editor. Drying of Porous Materials. Dordrecht, The Netherlands: Springer, 2007:29–42.
23. Chemkhi S, Jomaa W, Zagrouba F. Application of a coupled thermo-hydro-mechanical model to simulate the drying of nonsaturated porous media, *Drying Technol*. 2009;27(7–8):842–850.
24. Mihoubi D, Bellagi A. Drying induced stresses during convective and combined microwave and convective drying of saturated porous media. *Drying Technol*. 2009;27(7–8):851–856.
25. Kneule F. Drying. Warszawa: Arkady, 1970 (in Polish).
26. Kowalski SJ, Rybicki A. Rate of drying and stresses in the first period of drying. *Drying Technol*. 2000;18(3):583–600.
27. Kowalski SJ, Rybicki A. Cohesive strength of materials during drying processes, *Drying Technol*. 2009;27(7–9):863–869.
28. Kowalski SJ, Musielak G, Banaszak J. Heat and mass transfer during microwave-convective drying, *AIChE J*. 2010;56(1):24–35.
29. Kowalski SJ, Rajewska K, Rybicki A. Mechanical effects in saturated capillary-porous materials during convective and microwave drying. *Drying Technol*. 2004;22(10):2291–2308.
30. Kowalski SJ, Rajewska K, Rybicki A. Stresses generated during convective and microwave drying. *Drying Technol*. 2005;23(9–11): 1875–1893.
31. Kowalski SJ, Rybicki A. Qualitative aspects of convective and microwave drying of saturated porous materials. *Drying Technol*. 2004;22(10):1173–1189.
32. Kowalski SJ, Rajewska K. Drying induced stresses in elastic and viscoelastic saturated materials, *Chem Eng Sci*. 2002;57:3883–3892.
33. Musielak G. Possibility of clay damage during drying. *Drying Technol*. 2001;18(8):1645–1659.
34. Musielak G. *Modelling and Numerical Simulations of Transport Phenomena and Drying Stresses in Capillary-Porous Materials*. Poznań University of Technology, Poznań Transactions No 386, 2004 (in Polish).
35. Szarawara J. *Chemical Thermodynamics*. Warszawa: WNT-Scientific Technological Publishers, 1985 (in Polish).
36. Berry RS, Kazakov VA, Sieniutycz S, Szwast Z, Tsirlin AM. *Thermodynamic Optimization of Finite–Time Processes*. New York: Wiley, 2000.

Manuscript received Feb. 8, 2013, revision received May 28, 2013, and revision received Aug. 19, 2013.